Methanol carbonylation to acetaldehyde on Au particles supported by single-layer MoS2 grown on silica

Kortney Almeida[1], Katerina Chagoya[2], Alan Felix[2], Tao Jiang[3], Duy Le[3,4], Takat B Rawal[5], Prescott E Evans[6], Michelle Wurch[1], Koichi Yamaguchi[1], Peter A Dowben[6], Ludwig Bartels[1], Talat S Rahman[3,4] and Richard G Blair[4,7]

[1]Department of Chemistry and Materials Science & Engineering, University of California—Riverside
[2]Department of Mechanical and Aerospace Engineering, University of Central Florida
[3]Department of Physics, University of Central Florida
[4]Renewable Energy and Chemical Transformation (REACT) Cluster, University of Central Florida
[5]UT/ORNL Center for Molecular Biophysics, Oak Ridge National Laboratory
[6]Department of Physics and Astronomy, University of Nebraska
[7]Florida Space Institute, University of Central Florida

Abstract

Homogenous single-layer MoS_2 films coated with sub-single layer amounts of gold are found to isolate the reaction of methanol with carbon monoxide, the fundamental step toward higher alcohols, from an array of possible surface reactions. Active surfaces were prepared from homogenous single-layer MoS_2 films coated with sub-single layer amounts of gold. These gold atoms formed clusters on the MoS2 surface. A gas mixture of carbon monoxide (CO) and methanol (CH_3OH) was partially converted to acetaldehyde (CH_3CHO) under mild process conditions (308 kPa and 393 K). This carbonylation of methanol to a C_2 species is a critical step toward the formation of higher alcohols. Density functional theory modeling of critical steps of the catalytic process identify a viable reaction pathway. Imaging and spectroscopic methods revealed that the single layer of MoS_2 facilitated formation of nanoscale gold islands, which appear to sinter through Ostwald ripening. The formation of acetaldehyde by the catalytic carbonylation of methanol over supported gold clusters is an important step toward realizing controlled production of useful molecules from low carbon-count precursors.

Keywords

2D catalyst, MoS_2, gold, acetaldehyde, methanol, DFT

1. Introduction

The formation of higher alcohols from syngas is an important goal in the quest for economic and sustainable transformation of biomass into transportation fuels [1]. The production of methanol from syngas over copper is a well-understood reaction. The path toward higher carbon-count molecule is less understood. A necessary step for its realization is efficient C–C coupling involving oxygenate small molecules such as carbon monoxide and methanol [2, 3]. Important work by Haruta *et al* showed that CO oxidation is catalyzed by supported nanoscale gold particles [4]. This revealed that the catalytic activity of metals, that are relatively inert in the bulk, can be enhanced through nanostructuring [5]. Recently [6, 7], we have shown that gold nanoclusters deposited on single-layer molybdenum disulfide (MoS_2) coating can transform an otherwise inert substrate, silica, into a catalytic active surface for CO oxidation. This is similar to results obtained on reducible oxides, such as titania and ceria, decorated with gold nanoparticles [8–14]. Concomitant computational efforts have predicted a number of feasible, low-barrier reaction pathways on thus supported gold nanoparticles [6, 15], in contrast to the catalytically largely inactive bulk gold, gold on pristine silica, or on other 2D materials like graphene [16–18]. Here, we address the carbonylation of methanol as the most fundamental C–C coupling step that can lead to higher alcohol formation from a lower alcohol. The mixture of methanol and carbon monoxide was investigated as an approximation of the reaction stream from syngas over the catalysts surface; hydrogen, water and other species were excluded to maintain a system simple enough to model computationally. Syngas may be obtained from biomass gasification, and conversion to higher alcohols is a potential rapid pathway toward sustainable and renewable fuels.

Molybdenum disulfide has been investigated for a wide range of catalytic applications. MoS_2 with cobalt and alkali modifiers is the key catalyst material in industrial hydrodesulfurization; notably, the industrial catalyst material resembles a few-layer film of supported MoS_2. [19] Alkali modification of this material has also been proposed for alcohol formation [20–28]. Sulfur vacancy driven chemical activation of the basal plane of single layer MoS_2 has also been proposed [29]. The mechanistic aspects of these studies have focused on the hydrogenation step, in particular the initial CO hydrogenation to produced methanol. To further the understanding of catalysis over this material, our study focuses on the extension of the carbon chain (figure 1(a)) toward higher alcohols through the carbonylation of methanol.

MoS_2 has gained prominence as a catalyst for hydrogen evolution [30–34]. In earlier studies its activity was attributed to edge sites based on low-temperature measurements [35], and related materials that feature large number of exposed edge sites have been prepared and validated in some catalytic applications [29, 36–41]. It has been shown that MoS_2 support. In this work we have sought to investigate the interaction between the support and catalytically active nano clusters. By producing polycrystalline continuous single-layer MoS_2 coatings over several centimeter in diameter [42], we avoid any possible contributions from the edge sites and can focus solely on grain boundaries and metal-MoS_2 sites. This simplified structure allows us to probe the fundamental chemistry of chain lengthening.

In this article, we report surprising findings, based on experimental evidence and density functional theory (DFT) calculations, that the carbonylation of methanol is successfully catalyzed over the Au–MoS_2 structures to yield acetaldehyde and that using a laminar flow reactor, acetaldehyde formation occurred at fairly low temperatures (as low as 393 K), on single layer MoS_2 films, decorated by nanoscale gold islands. The rest of the article is organized as follows: experimental and computational methods are presented in section 2;

results and discussion, which summarize our main findings, are shown in section 3; and finally, conclusions are presented in section 4.

2. Materials and methods

2.1 Experimental details

A 1.5 cm × 1 mm thick fused silica window (Esco Optics) was homogeneously coated with a single polycrystalline layer of MoS_2 decorated by nanoscale gold islands corresponding to an average gold coverage of 0.5 Å, 1 Å, and 2 Å or approximately 1/6, 1/3, and 2/3 of a monolayer respectively. Figure 1(b) shows the preparative effort schematically and figure 1(c) depicts the fused silica window after single-layer MoS_2 and gold deposition.

To make the supported catalysts, we have utilized a technique for coating inert oxides by an MoS_2 film of controlled integer number of layers, as reported elsewhere [42]. The original work focused on MoS_2 films on a dry-oxide SiO_2 layer on a silicon wafer substrate. The single- and few-layer MoS_2 growth technique is based on heating molybdenum filaments to white heat (>1500 K) under high vacuum followed by exposure to carbon disulfide. Decomposition of the disulfide on the Mo filament surface results in volatile MoS_x precursors, which are precipitated onto the substrate. The substrate is held at a temperature where MoS_2 island growth and desorption is at equilibrium. The reference sample for scanning electron microscopy (SEM) and atomic force microscopy (AFM) was prepared on a thin (30 nm) silicon dioxide film on a doped silicon substrate. Gold was deposited with an e-beam evaporator monitored by a quartz crystal microbalance. Deposition rates were calculated from the measured mass increase and converted to Ångstroms of gold per minute. Values below the atomic diameter of gold (3.2 Å) indicate incomplete (sub-monolayer) coverage.

Reactor studies were performed in a laminar flow reactor, as shown in figures S1–S3 (https://stacks.iop.org/JPCM/34/104005/mmedia) in supplementary information (SI). The goal of this study was to determine the chain lengthening products from carbon monoxide addition to methanol. To this end reactions were run for 140 min at 150 ◦C. This allowed the product composition to stabilize and be analyzed in steady state. Product analyses were performed on two gas chromatographs: an Agilent 6890 with a wax column (Restek Stabilwax, 30 m, 0.32 mm ID, 1.0 μm film thickness) and a mass sensitive detector (Agilent 5973) was utilized for samples taken with a 25 ml gas tight syringe from a sampling port in the product stream. An Agilent 6850 gas chromatograph with a wax column (Restek Stabilwax, 30 m, 0.32 mm ID, 1.0 μm film thickness) and thermal conductivity detector (TCD) was connected directly to the product stream via a transfer line and a gas-sampling valve. The chromatographic methods and the laminar flow reactor are further described in the SI. Blanks were run with an empty reactor, with a blank fused silica substrate, and a MoS_2 coated substrate with no gold.

2.2 Calculation details

Our DFT calculations are based on the plane-wave basis set and pseudopotential method employing the generalized-gradient approximation in the form of the Perdew–Burke–Ernzerhof [43] functional together with DFT-D3 correction [44] to take into account both electron- exchange and van der Waals interactions. We used a cutoff energy of 500 eV for truncation of the plane-wave basis set. We sampled the Brillouin zone with one point at the

zone-center. We used Gaussian smearning with a width of 0.1 eV. We relaxed the systems using the standard minimization algorithm [45] until the residual force on each atom is below 0.01 eV $Å^{-1}$ and the total energy converges below 1×10^{-5} eV.

Our supercell model consists of a periodic (6 × 6) system of single layer MoS_2 using an optimized lattice constant of 3.16 Å, a vacuum of 25 Å, and Au_{13} nanoparticle adsorbed on one side of the MoS_2 sheet. To mimic defect-laden MoS_2 surface (with 1.5% defects), we removed one S atom from one side of the (6 × 6) MoS_2 basal plane. In this work, we considered only the lowest-energy structure of Au_{13}/ MoS_2 as previously obtained by Rawal et al [46].

Transition states and activation barriers reactions were calculated using the climbing-image nudged elastic band (CI- NEB) method [47, 48] with a force convergence threshold of 0.05 eV $Å^{-1}$. Note that before performing CI-NEB calculations, the initial minimum energy paths for each reaction were determined using the NEB method [47].

3. Results and discussion

3.1 Characterization of gold nanoparticles as deposited on MoS_2

The samples exhibited (figure 2(a)) the typical Raman peak positions for single-layer MoS_2 films for E_{2g} and A_{1g} modes at 385.5 cm^{-1} and 404.9 cm^{-1} (separation 19 cm^{-1}), respectively, consistent with earlier reports [49, 50]. Before gold deposition, the photoluminescence of the substrate material (figure 3) was intense and centered at 1.91 eV with a full-width at half-maximum of ~0.1 eV, the optical bandgap of single-layer MoS_2 [51, 52]. After gold deposition, the photoluminescence was quenched. This indicates that despite the incomplete surface coverage, there is a quenching center within the size of practically any exciton that is created on the surface. It also suggests efficient dispersion of gold on MoS_2/SiO_2, in contrast to gold on bare silica or graphene. Direct SEM imaging of a test sample with a 30 nm silica film on silicon shows tiny, point-like gold particles near the limit of the instrument's resolving power (figure 4). Image analysis showed that the majority of these particles range in size from diameters of 1–5 nm, i.e. in a useful size range for catalytic activity [53–55], and indicated that the nanoparticles are dispersed on the basal plane of MoS_2, unlike the case of Au nanoparticles decorating the edges of MoS_2 reported elsewhere [56]. The spatial homogeneity of the sample was verified by determining the Raman peak separation and photoluminescence position along a line across the substrate. The presence of Au particles on MoS_2/SiO_2 was also confirmed with the x-ray absorption spectroscopy published elsewhere [7, 57].

3.2 Synthesis of acetaldehyde

The reactant stream consisted of CO gas at 308 kPa bubbled through a methanol reservoir at 20 ◦C. At this temperature methanol has a vapor pressure of 13 kPa or 4.2% of the feed stream. Prior to the reaction, the reactor was purged with argon gas and heated to the reaction temperature of 150 ◦C.

After 120 min on stream, a sample was taken for GC-MS analysis by a sampling port. Comparison of the product peak with GC-MS chromatogram of a standard acetaldehyde/methanol mixture (figure S4) indicated that the observed peak in the TCD

chromatogram is acetaldehyde. Carbon monoxide (RT = 2.295 min), acetaldehyde (RT = 3.305 min), methanol (RT = 4.245 min) and water (RT = 5.149 min) were detected in TCD chromatograms. Water was detected in all reactions (with and without gold) at very low concentrations.

We investigated the stability of the catalyst by running the reactor for 140 min and reusing a catalyst after on stream. The 1 Å catalyst was utilized for 140 min, stored in an Ar-filled glovebox for 20 days and reused. Catalytic acetaldehyde formation was still observed. Figure 5 shows the production of acetaldehyde as a function of time on stream for all samples. While we observed a slight drop initially, in the production of acetaldehyde, we found that subsequently the reaction proceeds at a consistent rate. The delay in the onset of catalysis is related to the flow rate of the reactant stream. This was the time to purge the 13.4 cm^3 transfer line volume when switching from argon purge to reactant stream. The 2 Å sample had a higher reactant flow rate. A blank consisting of the MoS_2 coated substrate without gold did not produce measurable amounts of acetaldehyde. As estimation of number of active sites in our samples was not possible, we could not evaluate turnover frequency and turnover number for the catalyst.

3.3 Modeling of the C–C bond formation

Accompanying DFT calculations validate the feasibility of formation of carbon–carbon bonds at the surface of MoS_2-supported Au nanoparticles from carbon monoxide and methanol alone. Continuing the success of previous computational work [46], in which the alcohol synthesis from syngas (CO and H2) was shown to be favorable on Au_{13} nanoparticles stabilized by interactions with a single layer of MoS_2, and that, thanks to the inertness of MoS_2 support, reactions prefer not to occur at the interfacial sites between the particle and MoS_2 supports, we used the same supercell setup to study the formation of a bond between adsorbed methyl and carbonyl species to acetyl. We considered the formation of acetaldehyde by studying the most likely processes: $CH_3^* + CO^* \rightarrow CH^3CO^*$ and $CH_3CO^* + H^* \rightarrow CH_3CHO^*$, where CH_3^* and H^* species are produced through the adsorption and dissociation of methanol on the stabilized gold surface ($*$ designates adsorbed species). Additionally, CO is required to reduce residue O^* species via $O^* + CO^* \rightarrow CO_2^*$, a highly exothermic reaction ($\Delta E =$ 2.23 eV) with a barrier of 0.06 eV, as also described elsewhere [6, 7]. Figures 6(a) and (b) shows the initial state, transition state, and final states of the acetyl formation, $CH_3^* + CO^* \rightarrow CH_3CO^*$, and the hydrogenation of acetyl to acetaldehyde, $CH_3CO^* + H^* \rightarrow CH_3CHO^*$, reactions. The co-adsorption energy of in the initial state of the acetyl formation is found to be 3.42 eV, suggesting a strong and stable co-adsorption. It is consistent with the fact that the methyl group ($–CH_3$) is rarely seen in gas phase and is very active. We also found that the co-adsorption energy of the species in the initial state of the hydrogenation of acetyl to acetaldehyde is 2.25 eV, suggesting another stable co-adsorption structure. Our calculations indicate that the formation of a bond between the adsorbed CH_3^* species and a CO^* molecule on Au_{13} is energetically favorable as the reactions are exothermic and the activation barriers comparatively low: 0.69 eV for the acetyl formation (I) (figure 6(a)) and 0.47 eV for the hydrogenation of acetyl to acetaldehyde (II) (figure 6(b)). The resultant CH_3CHO^* is desorbs with a desorption energy of 0.45 eV. The atomic coordinates of all systems and raw computational data are available at Zenodo repository [58].

Close inspection of the energetics of the reaction pathways reveals that site with the lowest pathway barriers corresponds to the least coordinated gold atom on the cluster, for which the binding of the reactants is strongest. Such sites are far more common on small gold clusters.

Our finding highlights the importance of small clusters for this reaction to proceed. Furthermore, our work shows the efficacy of single-layer of MoS_2 to serve as a surface on which dispersal of gold into nanometer-scale clusters is favorable [15].

3.4 Gold nanoparticle catalyst sintering

Atomic force microscopy was used to analyze the effect of reaction on-stream time on the gold dispersion (figure 4). It was found that the as prepared gold particle size distribution from 1 to 5 nm (figure 7(a)) in diameter with a near exponential distribution suggestion random nucleation events, as seen in figure 7(a). The particles are shown to have circular shapes as the distribution of circularity is near unity (figure 7(b)).

After use for acetaldehyde production, the gold particles coalesced, resulting in Au particles with an increased diameter distribution centered near 40 nm (figure 7(c)). The change in distribution of the Au particle diameters to an exponential modified normal distribution (figure 7(c)) suggests the coalescing proceeds through Ostwald ripening mechanism. While the majority of the Au particles exhibit circularity ($4\pi(\text{area}/\text{perimeter}^2)$ is still near unity), after the production of acetaldehyde, a significant fraction show deviation toward elliptical shapes (figure 7(d)). This is also indicative of an Ostwald ripening mechanism.

Aggregation of gold particles is not unexpected as capped gold has been shown to behave similarly in solution experiments with temperatures over 120 ◦C [59] and platinum is predicted to have a high mobility on a MoS_2 surface [60].

4. Conclusions

In this work we have provided insights, through a merger of material preparation, experimental characterization and computational modeling, into intermediate steps in alcohol formation from syngas. We showed that the deposited gold nanoparticles on a single layer of MoS_2 on an inert fused silica substrate provide a catalyst surface capable of carbonylation of methanol to acetaldehyde at relatively low reaction temperatures and pressures (308 kPa and 393 K). The mechanism of the processes is illustrated by accompanying DFT calculations which reveal low activation barriers (~few tenths of an eV) and exothermicity of the C–C coupling elementary steps. This result showcases the promise of gold nanoparticles on single layers of MoS_2 as active catalysts even as the mean particle size increases during use.

More importantly, this work shows a promising way of preparing catalyst by utilizing a non-active support such as silica and the application of small amount of single layers of MoS_2 to support Au particles. More specifically, a mono-layer on 2 mm beads would be an equivalent MoS_2 loading of 1.88 ppm and an Au loading of 1.15 ppm. A cubic meter of supported catalyst prepared in such a way would require 146 mg of MoS_2 and 90 mg of gold. Furthermore, our results also speak to sustained reactivity of Au nanoparticles in a scenario in which inert substrates can first be shaped into desired structures that optimize reactant and heat flow and serve as an inexpensive scaffold for a composite that bestows catalytic activity on them.

Acknowledgments

We gratefully acknowledge joint funding from the United States Department of Energy Basic Energy Sciences grant DE-FG02-07ER15842 (UCF, UCR, UNL). We thank the

Advanced Research Computing Center at the University of Central Florida, and the National Energy Research Scientific Computing Center (NERSC) for providing the computer resources.

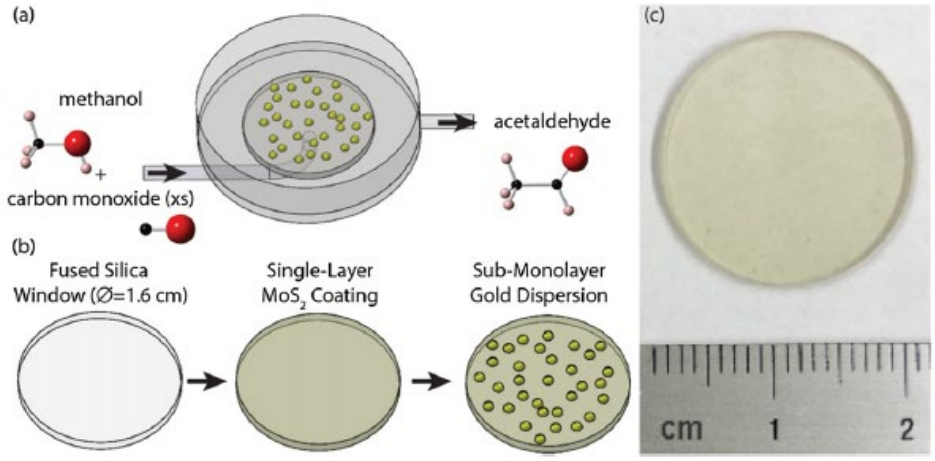

Figure 1. Schematic representation of the catalyst preparation and catalytic evaluation in a laminar flow reactor (a) and (b). The 1.5 cm fused silica window coated with a single-layer of MoS_2 and deposition of gold exhibits a yellowish color (c).

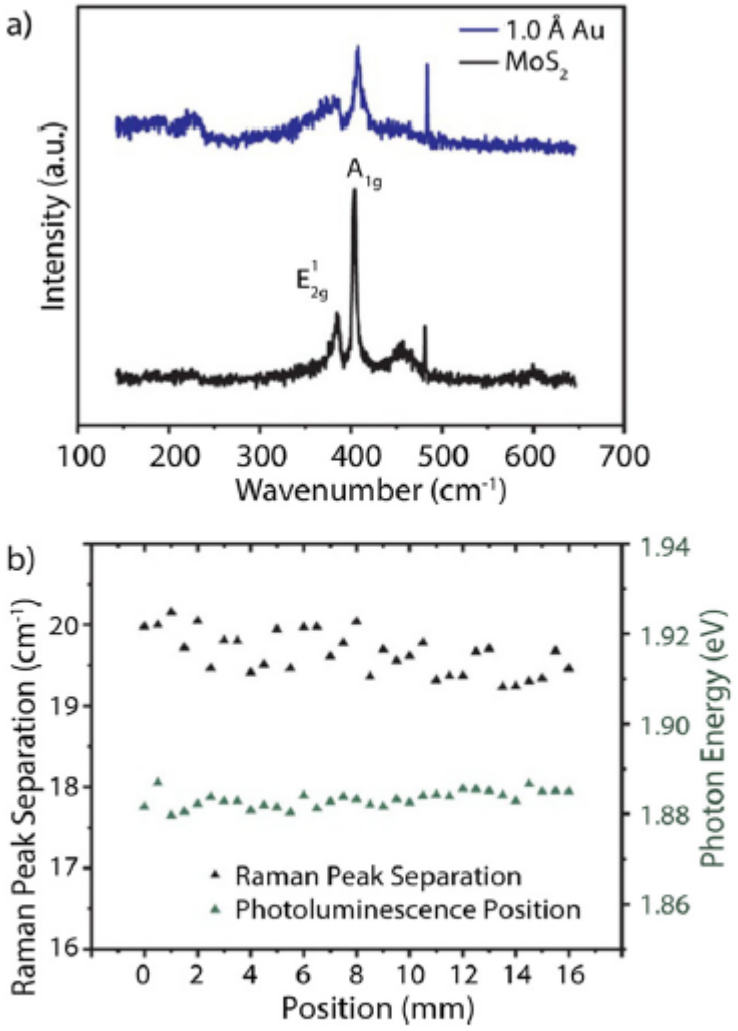

Figure 2. The Raman spectra of a single-layer MoS_2 sample before (black) and (color) after sub-monolayer gold deposition (a) and homogeneity of the single-layer MoS_2 film properties across the fused silica substrate before gold deposition (b).

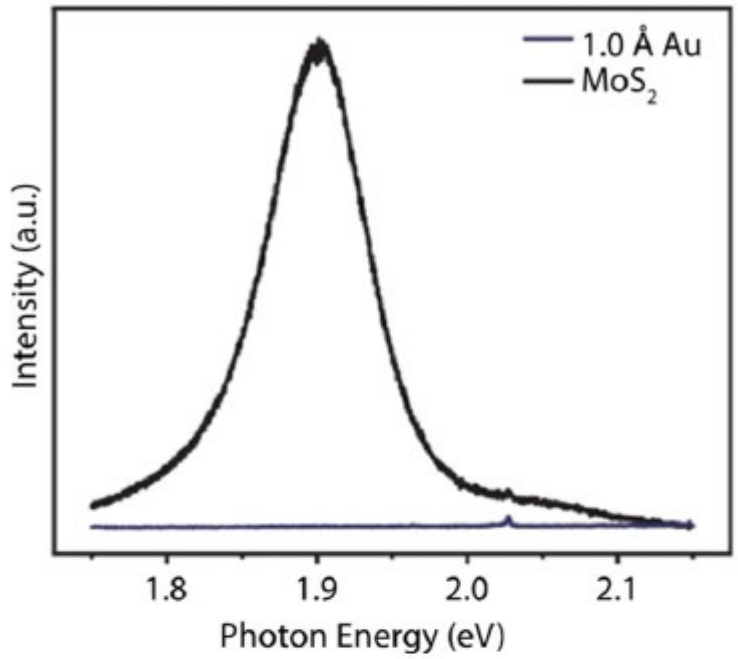

Figure 3. The photoluminescence of the deposited MoS_2 film before (black) and after gold deposition (blue) shows quenching by the gold particles and is used is a verification of deposition as well as homogeneity.

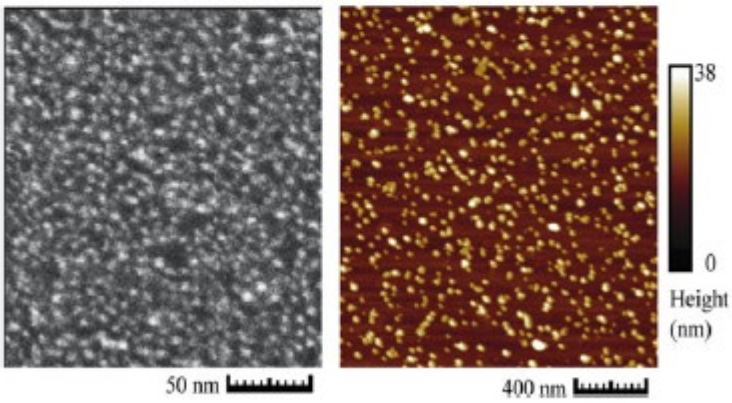

Figure 4. Initial deposition of Au, on a single layer MoS_2 film coating a 30 nm silica test film, produced well-dispersed particles ranging from 1–5 nm (SEM image, left). After two cycles on stream at 150 °C, a similarly coated sample shows particle agglomeration producing a distribution centered around 40 nm (AFM right).

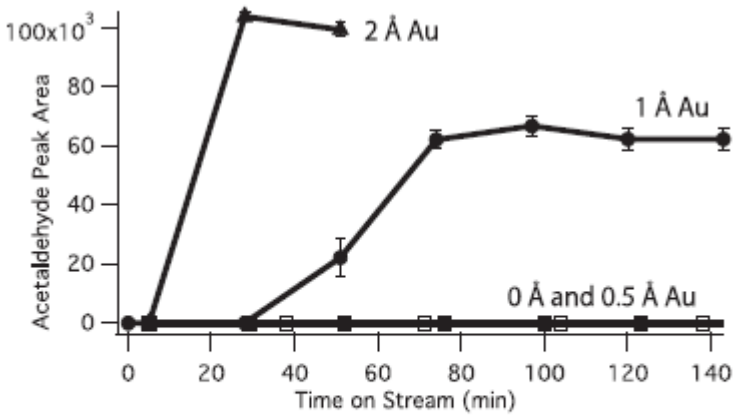

Figure 5. The integrated acetaldehyde peak intensity, as a function of the on-stream time at 150 °C, shows the onset of activity after a 20–30 min induction period. Time zero is when the reactor, at temperature, was switched from an argon to reactant feed.

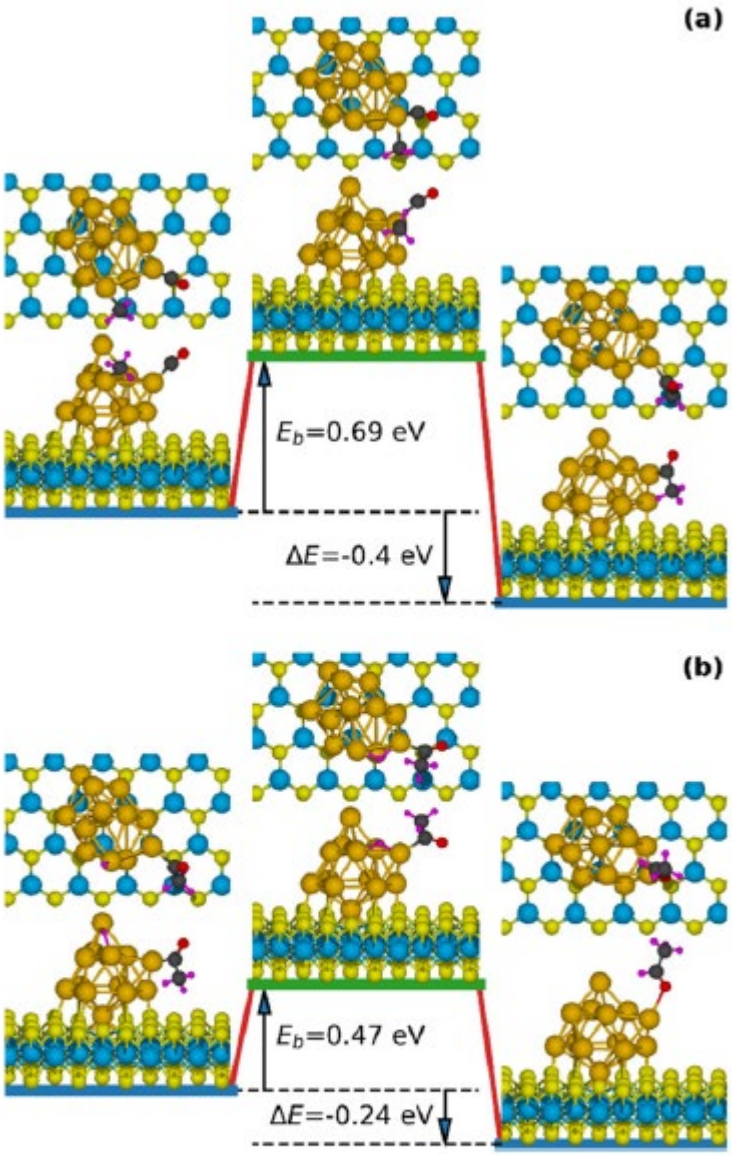

Figure 6. Reaction pathways of $CH_3^* + CO^* \rightarrow CH_3CO^*$ (a) and $CH_3CO^* + H^* \rightarrow CH_3CHO^*$ (b). Left, center, and right images show both top and side views of initial, transition, and final states, respectively. Blue, yellow, gold, black, red, and magenta balls represent Mo, S, Au, C, O, and H atoms, respectively. E_b and ΔE are activation barrier and reaction energy, respectively.

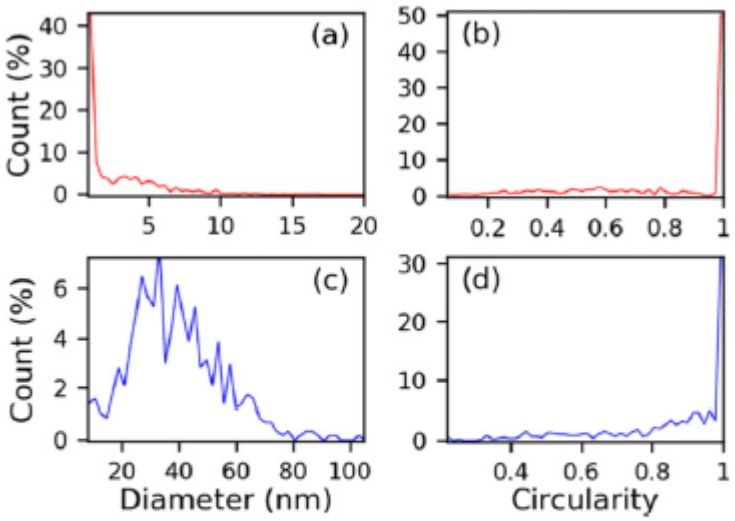

Figure 7. Distributions of diameter (a) and circularity (b) of gold particles as deposited on MoS_2 and those after use for acetaldehyde production shown in (c) and (d), respectively. Circularity is defined as 4π(area/perimeter^2).

References

[1] Grim R G, To A T, Farberow C A, Hensley J E, Ruddy D A and Schaidle J A 2019 *ACS Catal.* **9** 4145
[2] Bai H, Ma M, Bai B, Cao H, Zhang L, Gao Z, Vinokurov V A and Huang W 2019 *Phys. Chem. Chem. Phys.* **21** 148
[3] Choi Y and Liu P 2009 *J. Am. Chem. Soc.* **131** 13054
[4] Haruta M, Kobayashi T, Sano H and Yamada N 1987 *Chem. Lett.* **16** 405
[5] Hammer B and Norskov J K 1995 *Nature* **376** 238
[6] Rawal T B, Le D and Rahman T S 2017 *J. Phys. Chem.* C **121** 7282
[7] Almeida K *et al* 2019 *J. Phys. Chem.* C **123** 6592
[8] Haruta M, Tsubota S, Kobayashi T, Kageyama H, Genet M J and Delmon B 1993 *J. Catal.* **144** 175
[9] Schubert M M, Plzak V, Garche J and Behm R J 2001 *Catal. Lett.* **76** 143
[10] Deng W, De Jesus J, Saltsburg H and Flytzani-Stephanopoulos M 2005 *Appl. Catal.* A **291** 126
[11] Gardner S D, Hoflund G B, Schryer D R, Schryer J, Upchurch B T and Kielin E J 1991 *Langmuir* **7** 2135
[12] Chen M S and Goodman D W 2004 *Science* **306** 252
[13] Zhou Y *et al* 2013 *Angew. Chem., Int. Ed.* **52** 6936
[14] Yang F, Graciani J, Evans J, Liu P, Hrbek J, Sanz J F and Rodriguez J A 2011 J. Am. Chem. Soc. 133 3444
[15] Merida C S et al 2018 J. Phys. Chem. C 122 267
[16] Wang B and Bocquet M-L 2011 J. Phys. Chem. Lett. 2 2341
[17] Katsiev K et al 2014 Appl. Surf. Sci. 304 35
[18] Zheng J X, Wang L, Katsiev K, Losovyj Y, Vescovo E, Goodman D W, Dowben P A, Lu J and Mei W N 2013 Eur. Phys. J. B 86 411
[19] Hansen L P, Ramasse QM, Kisielowski C, Brorson M, Johnson E, Topsøe H and Helveg S 2011 Angew. Chem., Int. Ed. 50 10153
[20] Surisetty V R, Dalai A K and Kozinski J 2011 Appl. Catal. A 404 1
[21] Morrill M R, Thao N T, Shou H, Davis R J, Barton D G, Ferrari D, Agrawal P K and Jones C W 2013 ACS Catal. 3 1665
[22] Claure M T, Chai S-H, Dai S, Unocic K A, Alamgir F M, Agrawal P K and Jones C W 2015 J. Catal. 324 88
[23] Surisetty V R, Dalai A K and Kozinski J 2010 Appl. Catal. A 385 153
[24] Lv M, Xie W, Sun S, Wu G, Zheng L, Chu S, Gao C and Bao J 2015 Catal. Sci. Technol. 5 2925
[25] XieW, Zhou J, Ji L, Sun S, Pan H, Zhu J, Gao C and Bao J 2016 RSC Adv. 6 38741
[26] Luk H T, Mondelli C, Ferr´eDC, Stewart JAand P´erez-Ramírez J 2017 Chem. Soc. Rev. 46 1358
[27] Luk HT, Forster T,Mondelli C, Siol S,Curulla-Ferr´eD,Stewart J A and P´erez-Ramírez J 2018 Catal. Sci. Technol. 8 187
[28] Ao M, Pham G H, Sunarso J, Tade M O and Liu S 2018 ACS Catal. 8 7025
[29] Le D, Rawal T B and Rahman T S 2014 J. Phys. Chem. C 118 5346
[30] KimJ, Byun S, SmithA J,Yu J and Huang J 2013 J. Phys. Chem. Lett. 4 1227
[31] Osaki T, Narita N, Horiuchi T, Sugiyama T, Masuda H and Suzuki K 1997 J. Mol. Catal. A 125 63
[32] Chai B, Xu M, Yan J and Ren Z 2018 Appl. Surf. Sci. 430 523
[33] Askari M B, Beheshti-Marnani A, Seifi M, Rozati S M and Salarizadeh P 2019 J. Colloid Interface Sci. 537 186

[34] Salarizadeh P, Askari M B, Seifi M and Rozati S M 2019 J. Electroanal. Chem. 847 113198
[35] Besenbacher F et al 2008 Catal. Today 130 86 [36] Sun D et al 2012 Angew. Chem. 124 10430
[37] Kibsgaard J, Chen Z, Reinecke B N and Jaramillo T F 2012 Nat. Mater. 11 963
[38] Ho T A, Bae C, Lee S, Kim M, Montero-Moreno J M, Park J H and Shin H 2017 Chem. Mater. 29 7604
[39] Ma Q et al 2013 J. Phys.: Condens. Matter. 25 252201
[40] Ma Q et al 2014 ACS Nano 8 4672
[41] Le D and Rahman T S 2013 J. Phys.: Condens. Matter. 25 312201
[42] Almeida K et al 2018 ACS Appl. Mater. Interfaces 10 33457
[43] Perdew J P, Burke K and Ernzerhof M 1996 Phys. Rev. Lett. 77 3865
[44] Grimme S,Antony J, Ehrlich S and KriegH 2010 J. Chem. Phys. 132 154104
[45] Press W H, Teukolsky S A, Vetterling W T and Flannery B P 2007 Numerical Recipes (Cambridge: Cambridge University Press)
[46] Rawal T B, Le D and Rahman T S 2017 J. Phys.: Condens. Matter. 29 415201
[47] Henkelman G and J´onsson H 2000 J. Chem. Phys. 113 9978
[48] Henkelman G, Uberuaga B P and J´onsson H 2000 J. Chem. Phys. 113 9901
[49] Lee C, Yan H, Brus L E, Heinz T F, Hone J and Ryu S 2010 ACS Nano 4 2695
[50] Singh A K, Pandey R K, Prakash R and Eom J 2018 Appl. Surf. Sci. 437 70
[51] Mak K F, Lee C, Hone J, Shan J and Heinz T F 2010 Phys. Rev. Lett. 105 136805
[52] Splendiani A, Sun L, Zhang Y, Li T, Kim J, Chim C-Y, Galli G and Wang F 2010 Nano Lett. 10 1271
[53] Valden M, Lai X and Goodman D W 1998 Science 281 1647
[54] Lopez N, Janssens T V W, Clausen B S, Xu Y, Mavrikakis M, Bligaard T and Norskov J K 2004 J. Catal. 223 232
[55] Bondzie V A, Parker S C and Campbell C T 1999 Catal. Lett. 63 143
[56] Park B, Lee D, Kim H-s., Cho Y, Park S, Kim C, Lee T,Woo D H and Kim J H 2020 Appl. Surf. Sci. 532 147486
[57] Merida C S et al 2017 J. Phys. Chem. C 122 267
[58] Almeida K et al 2021 Supplementary data for “Methanol carbonylation to acetaldehyde on Au particles supported by single-layer MoS2 grown on silica” Zenodo repository (https://doi.org/10.5281/zenodo.5787638)
[59] Sahu P and Prasad B L V 2014 Langmuir 30 10143
[60] Saidi W A 2015 Cryst. Growth Des. 15 642